Honeycomb-like porous 3D nickel electrodeposition for stable Li and Na metal anodes

Xu, Yaolin; Menon, Ashok Sreekumar; Harks, Peter Paul R.M.L.; Hermes, Dorothee C.; Haverkate, Lucas A.; Unnikrishnan, Sandeep; Mulder, Fokko M.

DOI
10.1016/j.ensm.2017.11.011

Publication date
2018

Document Version
Accepted author manuscript

Published in
Energy Storage Materials

Honeycomb-like porous 3D nickel electrodeposition for stable Li and Na metal anodes

Yaolin Xu,[a] *Ashok Sreekumar Menon,*[a,b] *Peter Paul R. M. L. Harks,*[a] *Dorothee C. Hermes,*[b] *Lucas A. Haverkate,*[b] *Sandeep Unnikrishnan,*[b] *Fokko M. Mulder*[a *]

[a] Materials for Energy Conversion and Storage (MECS), Department of Chemical Engineering, Faculty of Applied Science, Delft University of Technology, Van der Maasweg 9, 2629 HZ Delft, The Netherlands

[b] Holst Centre, Dutch national institute for applied scientific research (TNO), High Tech Campus 31, 5656 AE Eindhoven, The Netherlands

* Corresponding Author. Email: F.M.Mulder@tudelft.nl

Abstract

Li and Na metals have the highest theoretical anode capacity for Li/Na batteries, but the operational safety hazards stemming from uncontrolled growth of Li/Na dendrites and unstable electrode-electrolyte interfaces hinder their real-world applications. Recently, the emergence of 3D conductive scaffolds aimed at mitigating the dendritic growth to improve the cycling stability has gained traction. However, while achieving 3D scaffolds that are conducive to completely prevent dendritic Li/Na is challenging, the routes proposed to fabricate 3D scaffolds to date are often complex and expensive. This not only leads to sub-optimal battery performance but can make the manufacturing nearly unachievable, compromising their commercial viability. We herein introduce a facile and single-step route to honeycomb-like 3D porous Ni@Cu scaffolds via a hydrogen bubble dynamic template (HBDT) electrodeposition method. The current collectors fabricated by this method offer highly stable cycling performance of Li plating/stripping (> 300 cycles at 0.5 mAh cm^{-2} and over 200 cycles at 1.0 mAh cm^{-2}), attributed to their ability to effectively accommodate Li/Na deposits in their porous networks and to delocalize the charge distribution. The beneficial role of $LiNO_3$ as an electrolyte additive in improving the mechanical integrity of solid electrolyte interface (SEI) and mechanistic insights into how the 3D porous structure facilitates Li/Na plating/stripping are comprehensively presented. Finally, with an outstanding cycling performance of reversible Na deposition (over 240, 110 and 50 cycles for 0.5, 1.0 and 2.0 mAh cm^{-2} at 1.0 mA cm^{-2}), our findings open new doors to expedite the development of Li/Na metal battery technology.

Graphical abstract

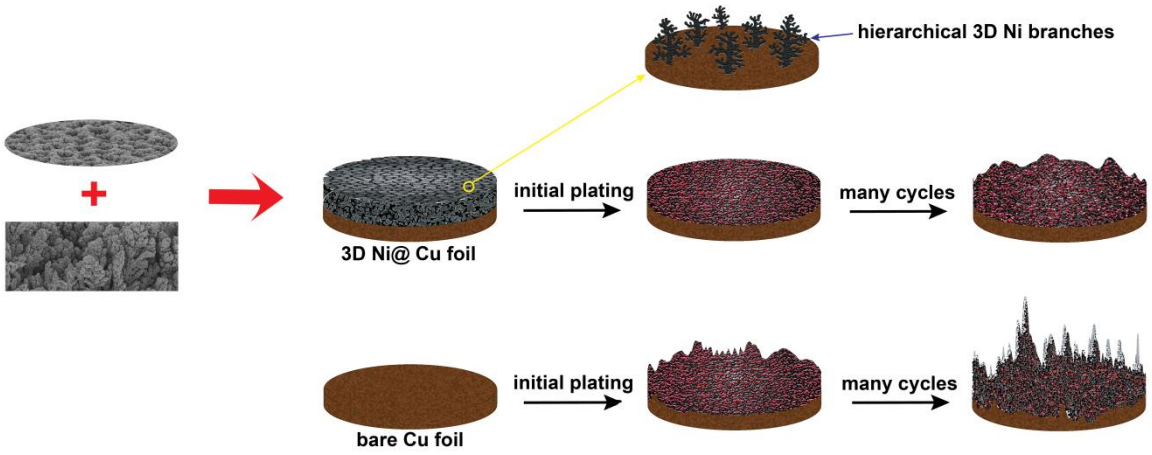

A facilely-synthesized, honeycomb-like 3D porous Ni@Cu current collector exhibits an outstanding cycling performance for Li/Na plating and stripping by accommodating the volume change in the porous host and suppressing the dendritic Li/Na growth.

Key words: Electrodeposition; 3D Nickel; Dendrite-free; Li/Na metal anode

Highlights

- A honeycomb-like 3D porous Ni@Cu current collector is facilely fabricated through a hydrogen bubble dynamic template (HBDT) electrodeposition method.
- A stable cycling performance for both Li and Na plating/stripping has been achieved.
- Effective suppression of the SEI formation upon $LiNO_3$ addition is comprehensively studied.
- The Li/Na nucleation mechanism in the porous honeycomb structure is reported.

1. Introduction

Energy storage is one of the key issues of modern society, and the Li metal anode is regarded as the "Holy Grail" of energy storage systems which offers an extremely high theoretical capacity of 3860 mAh g^{-1} and superior electrochemical reduction potential of -3.04 V *vs.* standard hydrogen electrode. Because of these figures-of-merit, Li metal anodes were intensely investigated in the early 1980s but sooner the efforts were largely stymied due to observations where the dendritic growth of Li constituted serious safety hazards. But the ongoing research on high-capacity cathode materials based rechargeable battery systems, such as Li-O_2 and Li–S batteries, in order to cope with the increasing energy storage density demand, has recognized the imperative of revisiting this once-abandoned research [1-5]. Meanwhile, driven by the limited and uneven distribution of global lithium resources in addition to the higher abundance and lower cost of Na compared to Li, Na metal batteries have also attracted considerable research interest [6-8].

However, the Li dendrite formation that is fatal to battery operation has largely hindered the practical application of high-energy-density metal anodes. The formation of dendrites is caused by inhomogeneous distribution of current density on the metal anode and generation of charge concentration gradient at the electrolyte/electrode interface [2-4]. Dendrites are tapered branch-like structures that grow out from the anode during cycling [9], which gives rise to several plaguing issues [2-5], such as (1), serious safety concerns which arise when the dendrites penetrate through the separator and come into physical contact with the cathode, which leads to short-circuit of the batteries; (2), the virtually infinite volume expansion owing to its host-less nature that exerts a formidable stress on the solid electrolyte interphase (SEI) layer, leading to the mechanical instability of the SEI layer and low Coulombic efficiency, and when the porous dendritic Li growth occurs this aggravates the problem; (3), the creation of "dead Li" due to the unstable interfacial chemistry, which are basically electrically isolated

Li metal generated after repetitive cycling resulting in the loss of active materials and thus the capacity decay. In short, the Li dendrite formation not only jeopardizes the safe operation of Li metal batteries, but also results in a low Coulombic efficiency and limited cycle life. With similar phenomena plaguing Na metal anodes, the progress towards Na metal batteries is also hampered.

In the pursuit of a dendrite-free Li metal anode, different methodologies have been developed to mitigate the above issues. There are many approaches undertaken including Li metal electrodes with engineered surfaces [10-15] and structures [16-24], structured current collectors [25-38], modified electrolytes [39-47] and separators [48-50]. Among these, 3D conductive host matrices attract the most research interest [21-37] because they hold promise for acting as a scaffold that can accommodate the volume changes whilst ensuring a more homogeneous charge distribution, and thus warranting an improved cycling performance. This can be attributed to the large surface area, which, according to Sand's model, can delay the initial growth of dendrites [2, 5, 51, 52]. Of particular interest are metallic 3D scaffolds which are more promising because of their increased electronic conductivity and mechanical stability. Many 3D structured hosts have been explored including various 3D porous Cu substrates [27-30], free-standing Cu nanowires [31], lithiophilic Cu-Ni core-shell nanowires [24], and 3D graphene@Ni scaffold [32] to name a few. The Cu-Ni core-shell network was prepared through the solution-based synthesis of Cu nanowires onto which Ni was electrodeposited [24]. The 3D porous Cu substrates were prepared from routes e.g. H_2 reduced CuO nanocluster [27] or de-alloying of Cu-Zn alloy [30]. The free-standing Cu nanowires were prepared through a solvent evaporation assisted assembly technique [31]. These 3D porous metallic structures exhibit high mechanical strength and extremely high surface area, ensuring homogeneous charge distribution during Li plating/stripping and pronounced cycling stability of Li metal anode. However, most of these approaches are

advanced, complex and costly, which largely limits their commercial viability. Although these efforts have yielded optimistic and encouraging results, with immense scope for further improvement, the commercial realization requires a facile, fast and scalable manufacturing method, which is still to be developed.

On the other hand, sodium metal battery research is still in its infancy but is rapidly evolving since the beginning of this decade. This is mainly motivated by the scarcity of Li and abundancy of Na and therefore the development of Na metal batteries could be a timely substitute to meet the electricity storage challenge.

Similar to the studies on Li metal anodes, research on metallic Na anodes also involve different approaches, including modified electrolytes [53-55], surface coating [56-58], 3D host structures [59] and engineered current collectors [60]. For instance, Luo et al. [59] developed carbonized wood with vertical channels as a scaffold for Na metal, which achieves a high cyclability over 500 h at 1.0 mA cm^{-2} but involves a relatively complex fabrication process. Cohn et al. [60] developed a nanocarbon nucleation layer on Al current collector which exhibits a high cycling stability over 1000 plating/stripping cycles, but it was cycled at a low current rate (0.5 mA cm^{-2}) and with a low Na loading (0.25 mAh cm^{-2}).

In this work we introduce a honeycomb-like hierarchical 3D porous nickel electrodeposition on a plain Cu substrate, which is facilely synthesized with a one-step, rapid (~ 30 s) hydrogen bubble dynamic template (HBDT) electrodeposition method [61], fabricating high performance current collectors for both Li and Na metal anodes. The 3D Ni@Cu current collector exhibits excellent electrochemical performance for reversible Li plating/stripping (> 300 cycles at 0.5 mAh cm^{-2} and over 200 cycles at 1.0 mAh cm^{-2} cycling at 1.0 mA cm^{-2}); the effect of $LiNO_3$ additive in the electrolyte has been comprehensively studied and the Li plating mechanism in the porous host has been unveiled. These electrodes also show outstanding cycling performance of Na plating/stripping (stable over 240, 110 and 50 cycles

for 0.5, 1.0 and 2.0 mAh cm^{-2} at 1.0 mA cm^{-2}). Thus, our newly-engineered current collectors may serve as an efficient solution to suppress the detrimental dendrite formation, enabling stable Li and Na metal anodes, as illustrated in **Fig. 1**.

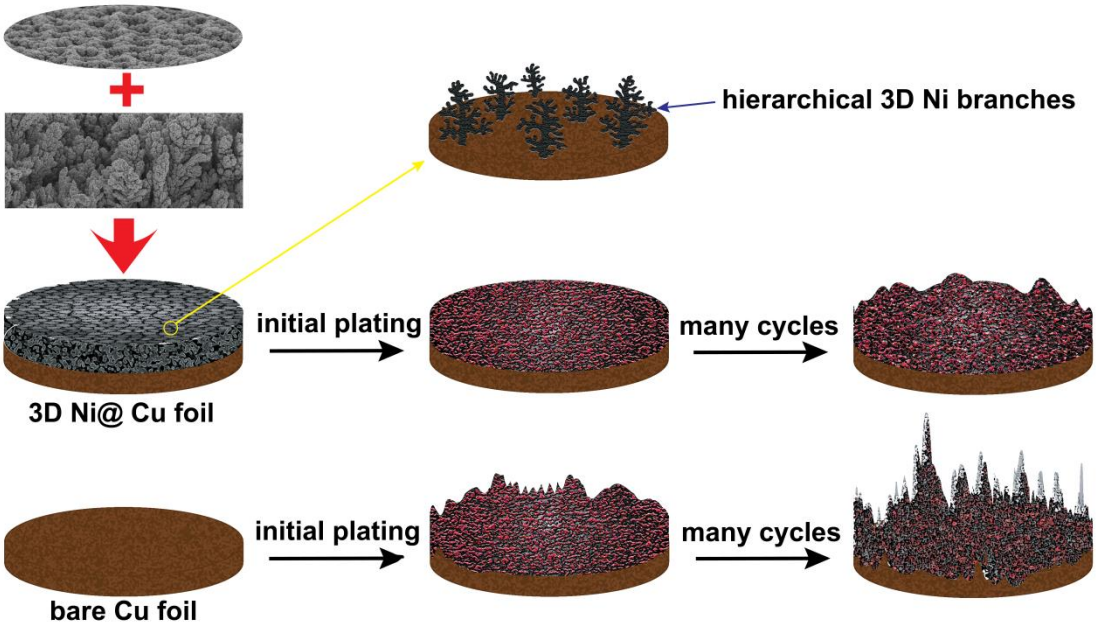

Fig. 1. A schematic of the Li/Na plating process on a honeycomb-like 3D Ni@Cu and a planar Cu foil.

2. Methods

2.1 Current collector preparation

The 3D Ni@Cu current collector was prepared by galvanostatic electrochemical deposition using the HBDT method. A simple two-electrode setup (**Fig. S1**) was used, in which the working electrode was a polished Cu foil and the counter electrode was a Ni foil. The base electrolyte was prepared with 0.12 M $NiSO_4 \cdot 6/7H_2O$ and 1.5 M NH_4Cl dissolved in deionized water. The electrodeposition was carried out at room temperature and the size of the 3D Ni@Cu is 1 cm x 1 cm. The experimental setup and details of the electrodeposition process are provided in the **Supporting Information (SI)**.

The 3D Ni@Cu is prepared by electrodepositing nickel at 3.0 A cm^{-2} for 30 s using polyethylene glycol (PEG) 4000 as a surfactant additive in the base electrolyte, and the concentration of PEG was fixed at 100 mg per 300 mL electrolyte solution. The as-synthesized 3D Ni@Cu samples were dried in a vacuum oven (60 ^{o}C) overnight before the electrochemical measurement.

To control the characteristics of the 3D nickel deposition layer, various deposition parameters can be adjusted including the concentration of PEG additive (**Fig. S2**), electrodeposition duration (**Fig. S3**) and current density (**Fig. S4)** and protective post-deposition (**Fig. S5**). We noted that a number of possibilities in other applications can be envisioned when appropriate modifications to the nickel electrodeposition have been made [61]. Detailed discussions are included in the SI.

2.2 Electrochemistry measurement

Li/Na ion symmetrical cells were assembled inside an Ar-filled glove box (O_2 and H_2O: < 0.1 ppm). The 3D Ni@Cu (or reference bare Cu foil) was used as the working electrode and a Li/Na metal foil worked as the counter electrode, and one piece of celgard® 2400 separator wetted with liquid electrolyte was inserted in between.

In the Li cells, 1 M bis(trifluoromethylsulfonyl)amine lithium salt (LiTFSI) dissolved in 1,2-dimethoxyethane (DME) and 1,3-Dioxolane (DOL) (DME : DOL = 1:1 in volume) with or without 1 wt. % $LiNO_3$ was utilized as the electrolyte. For Na cells, the working electrolyte was 1 M Sodium hexafluorophosphate ($NaPF_6$) in diethylene glycol dimethyl ether (DEGDME).

The galvanostatic electrochemical performance were evaluated using a Maccor 4600 battery cycler at room temperature. The cells were firstly cycled within 0.01 and 1.0 V at 50 μA cm^{-2} for five cycles to remove surface contaminations and to stabilize the interface, after which the electrochemical Li/Na plating and stripping was carried out. The plating process was

terminated when a targeted capacity was reached; and a cut-off voltage of 0.5 V was applied for Li/Na stripping process. Electrochemical impedance spectroscopy (EIS) was performed using a PGSTAT302N Autolab within a frequency range between 100 kHz and 0.1 Hz.

2.3 Characterization

X-ray diffraction (XRD) was carried out with a PANalytical X'Pert Pro PW3040/60 diffractometer with Cu K_α radiation and the working voltage and current were 45 kV and 40 mA, respectively. Micro-morphological images were taken with a JEOL JSM 6010F scanning electron microscope (SEM) working at 10 kV.

3. Results and discussions

3.1 Characterization on the current collector

XRD patterns of the 3D Ni@Cu **(Fig. 2a)** demonstrate that, apart from the peaks from the underlying Cu foil, all the other diffraction peaks can be assigned to crystalline nickel, which is in line with the SEM based EDX (Energy-dispersive X-ray spectroscopy) analysis (**Fig. S6**). Rietveld refinement on the XRD patterns (**Fig. S7** and **Table S1**) suggests that the average crystalline domain size of nickel is around 19.1 nm calculated based on Scherrer equation using a Lorentzian broadening.

Fig. 2b – 2e shows that the as-synthesized 3D Ni@Cu appears as a honeycomb-like porous nickel layer on a Cu substrate. The walls of the honeycombs are made up of vertically-grown hierarchical nickel branches, of which the nickel particles are arrayed into a cauliflower-like nanosized spherical morphology. The thickness of the nickel deposition is about 30 μm, and it reaches ~ 50 μm when the nickel electrodeposition duration is doubled to 60 s (**Fig. S3**).

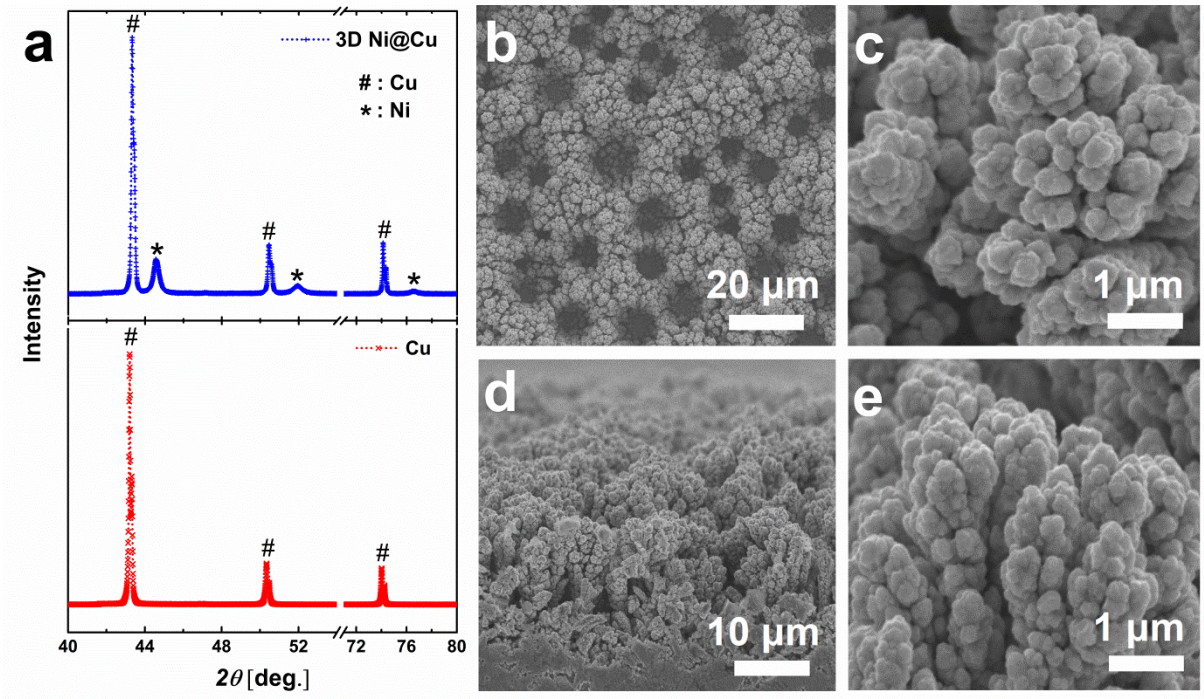

Fig. 2. Characterization on the as-synthesized 3D Ni@Cu. (a), XRD patterns .(b) – (c), top view and (d) - (e), cross-sectional SEM images.

Polyethylene glycol (PEG) is a common additive in the electrodeposition process [62], which works as a surfactant to reduce the surface tension between the gas-liquid (H_2 - electrolyte) interface in order to inhibit the coalescence of the bubble resulting in reduced bubble sizes and thus smaller pore sizes in the electrodeposition layer. The overall porosity of the 3D nickel layer, calculated based on the Faradaic efficiency, amounts to 81.7 % (details in the SI). Such a high porosity is more favorable to accommodate the substantial volume expansion upon Li deposition. Moreover, the estimated volumetric and gravimetric capacities of a Li metal anode with such nickel scaffold is significantly higher than a commercial graphite anode (**Table S2 & S3**).

3.2 Li deposition

3.2.1 Electrochemical performance & effects of $LiNO_3$

Li-ion cells were assembled using either a planar Cu foil or 3D Ni@Cu as the working electrode and Li metal foil as the counter electrode; and the Coulombic efficiency and voltage

hysteresis are measured as the benchmark to evaluate the reversible Li plating/stripping performance.

As shown in **Fig. 3a – 3b**, cycling at 1.0 mA cm^{-2} in a LiTFSI (without $LiNO_3$) based electrolyte, the cycling performance is found to be stable with a Coulombic efficiency of > 96 % over 300 cycles for an areal capacity of 0.5 mAh cm^{-2}; and a high performance can be retained for ~140 cycles when the capacity increases to 1.0 mAh cm^{-2}. When the Li deposition increases to 3.0 mAh cm^{-2}, the 3D Ni@Cu can still achieve a stable Coulombic efficiency above 97 % for ~ 60 cycles (**Fig. S8a – S8b**).

It should be noted that the initial Coulombic efficiency (without $LiNO_3$ addition) is low (43.8 % and 45.4 % for a capacity of 0.5 and 1.0 mAh cm^{-2}, respectively), which may originate from the substantial irreversible SEI formation due to the porous nature of the nickel layer that presents a large surface area; and the limited intrinsic kinetics of Li-ion diffusion may also play a role. **Fig. S8c** shows that the Coulombic efficiency improves when Li is stripped at a much lower current rate (0.1 mA cm^{-2}), indicating that the limited Li-ion diffusion kinetics accounts for the low Coulombic Efficiency during initial cycles. Nevertheless, the improvement in Coulombic efficiency is rather limited compared to the large amount of accumulated irreversible capacity during the previous cycles, suggesting that the unstable and thus continuous irreversible SEI formation plays a major role in the efficiency loss in the initial cycles. **Fig. S8c** also shows that, after about 140 cycles, the Coulombic efficiency drops drastically but a short-circuit (i.e. infinite plating process) does not happen. When the current density of Li stripping is set at 0.1 mA cm^{-2} (at the 168^{th} cycle) a large amount of Li can be stripped leading to an apparent high Coulombic efficiency of 159.3 %. It indicates that a substantial amount of lithium suffers from limited Li-ion transport over cycling possibly by the accumulated SEI layer on the electrode, but it is possible to recover partially.

To suppress the SEI formation and to enhance the mechanical stability of the SEI layer, $LiNO_3$ has been commonly applied as an additive in the electrolyte, which has been previously employed in Li-S systems to produce a stable interface layer on the Li metal in order to inhibit the problematic polysulfide shuttle [63, 64]. The positive effects of $LiNO_3$ as well as other nitrates such as KNO_3 in suppressing the dendritic Li deposition have also been reported [65]. In the initial cycle, $LiNO_3$ decomposes and reacts with Li to form a uniform and stable SEI film on the Li metal surface and prevents further SEI growth. From **Fig. 3c** it can be observed that, when 1 wt. % $LiNO_3$ is added into the electrolyte, the initial Coulombic efficiency increases to 92.9 % and remains above 96 % over 200 cycles. **Fig. S8d** shows that, when cycling at a high current density of 5.0 mA cm^{-2}, the Coulombic efficiency is practically stable over 90 cycles. Compared with the performance in an electrolyte without $LiNO_3$, the remarkable improvement in both Coulombic efficiency and cycling stability points to the formation of a more stable SEI layer upon $LiNO_3$ addition.

The positive effects of $LiNO_3$ addition in the electrolyte is also supported by the galvanostatic voltage profiles (**Fig. 3d – 3f**) and EIS spectra (**Fig. 3g – 3i**). It is observed that the charge transfer resistance of the bare Cu electrode grows gradually over cycling and so does the voltage hysteresis between charge and discharge. In comparison, the 3D Ni@Cu electrode exhibits a much lower charge transfer resistance but with an increasing voltage hysteresis (without $LiNO_3$ addition). The gradual increase of resistance for both cases roots in the continuously growing SEI layer. However, when $LiNO_3$ is added, the initial resistance during Li plating is higher than that using a $LiNO_3$-free electrolyte due to the presence a compact, non-conductive SEI layer and therefore a higher nucleation energy barrier, but the resistance remains stable over cycling. The voltage hysteresis halts at ~ 120 mV after 100 cycles (compared with 179 mV after 100 cycles in a $LiNO_3$-absent electrolyte) illustrating that the SEI stabilizes after the first cycle and further growth is negligible. Moreover, when the

cycling rate increases from 1.0 to 5.0 mA cm^{-2}, the voltage hysteresis between charge and discharge merely increases by ~ 50 mV (**Fig. S8e**) indicating that the DC resistance of the $LiNO_3$ based SEI layer is basically low, which is also consistent with the previous report [65]. To further understand the role of the $LiNO_3$ during cycling, the evolution of the morphology and chemical composition of the SEI layer is studied with SEM, XRD and X-ray photoelectron spectroscopy (XPS) techniques. SEM images of the 3D nickel electrodes (**Fig. 3j – 3p**) reveal that, cycling in an electrolyte without $LiNO_3$, the surface of the nickel layer has been covered by a distinct SEI stratum after merely 5 cycles which thickens over cycling, and consequently, the resistance and overpotential increases. In comparison, the SEI layer on the electrode cycled in a 1 wt.% $LiNO_3$-LiTFSI based electrolyte is hardly noticeable after 5 cycles and only a thin and fluffy interphase layer is formed after 50 cycles suggesting the significant suppression of SEI growth and hence a stabilized low resistance due to the presence of a stable SEI layer. This is in good agreement with the voltage and EIS analysis. XRD patterns (**Fig. S9**) show that no peaks belonging to the SEI layer can be observed, indicating that it is amorphous; meanwhile, the peak intensity of the nickel phase reduces after cycling owing to the coverage of the SEI layer, and the reduction is more pronounced using a $LiNO_3$-free electrolyte. It reveals that the $LiNO_3$ has effectively controlled the SEI formation resulting in a much thinner SEI layer, which is consistent with the micrographs. XPS spectra (**Fig. S10**) indicate that the SEI layer formed in a pure LiTFSI based electrolyte consists of Li_2CO_3, Li_2O, $R_3COLi–(CH_2)–$, $R_3CO–R$, Li_xSO_y, LiF and Li_2S_x, etc. [66-69] originating from the decomposition of LiTFSI salt and DME/DOL solvents. In comparison, the SEI grown in a 1 wt.% $LiNO_3$-LiTFSI based electrolyte contains $R_3CO–R$, Li_xNO_y, Li_xSO_y and LiF, etc. [66-69], and remarkably no Li_2CO_3, Li_2O, $R_3COLi–(CH_2)–$ and Li_2S_x is observed. It also verifies the suppressed SEI formation due to the presence of $LiNO_3$ which first

decomposes and forms a stable and compact Li_xNO_y based layer and ultimately inhibits the continuous progression of SEI growth.

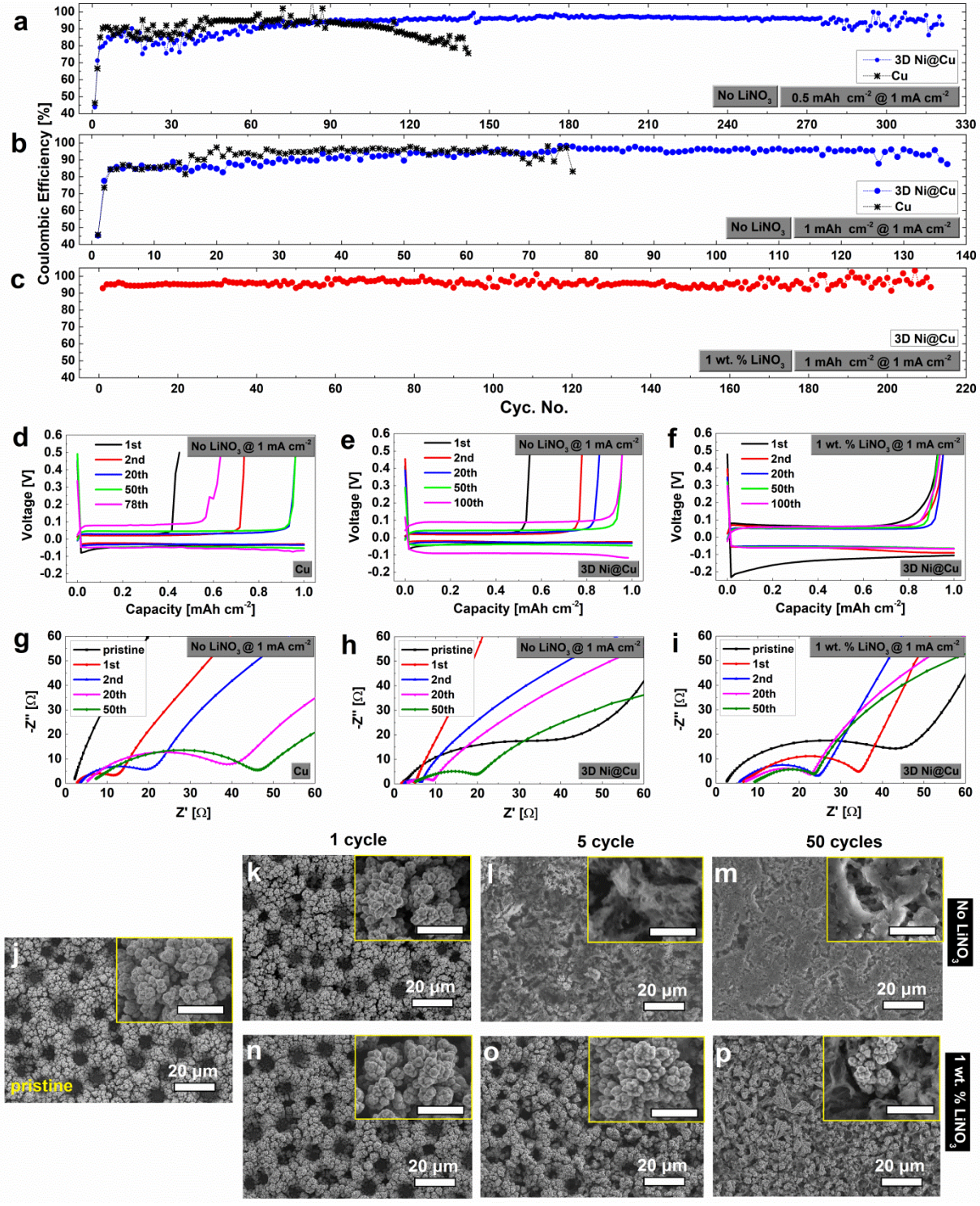

Fig. 3. Performance of the planar Cu and 3D Ni@Cu for reversible Li deposition and the morphological evolution of 3D Ni@Cu during cycling. (a) – **(c)**, Cycling performance, **(d)** – **(f)**, Cycling voltage profiles and **(g)** – **(i)**, EIS spectra of bare Cu and 3D Ni@Cu electrode

for Li plating and stripping cycling at 1 mA cm^{-2}. Here the capacity of Li deposition is fixed at 0.5 mAh cm^{-2} in Fig. (a) and 1.0 mAh cm^{-2} in all the other figures. **(j)** – **(p)**, SEM images of the 3D Ni@Cu electrodes: (j), pristine; (k) – (m), after 1, 5 and 50 cycles in the $LiNO_3$-free electrolyte; (n) – (p), after 1, 5 and 50 cycles in the $LiNO_3$-containing electrolyte. In Fig. (k) – (p), the capacity is fixed at 1.0 mAh cm^{-2} and the applied current density is fixed at 1.0 mA cm^{-2}. Length of the scale bars in the insets: 500 nm.

Based on the observations in **Fig. 3** and **Fig. S8 - S10**, we can conclude that the failure mechanism of the 3D Ni@Cu current collector for Li plating/stripping roots in the following aspects: (i), when a $LiNO_3$-free electrolyte is used, the unstable and thus continuous SEI growth results in a low Coulombic efficiency and the accumulation of non-conductive interphase that increases the internal resistance and overpotential. (ii), using a $LiNO_3$-containing electrolyte, the Coulombic efficiency has been significantly promoted (> 96% over 200 cycles) but still indicates that a minor fraction of the deposited Li is not recovered during stripping. For both (i) and (ii), the limited Coulombic efficiency may originate from the long Li diffusion pathway in the nanopores of the nickel host, apart from the finite intrinsic Li diffusion kinetics. This problem will be aggravated when a higher cycling current density and/or a higher Li deposition capacity is applied. (iii), the mechanical strength of the nickel structure appears to be limited over repetitive Li plating and stripping (**Fig. 3p**), which needs to be improved to maintain the structural integrity of the electrode to prolong its cycle life.

3.2.2 Li plating mechanism

To elucidate the mechanism of Li plating in the 3D nickel structure, micro-morphologies of the Li deposits under varying current densities and with different capacities were *ex-situ* imaged, as shown in **Fig. 4** and **Fig. S11**.

Depositing a fixed amount of Li (0.5 mAh cm^{-2}) at various current rates, the increasing current density results in reduced Li nuclei sizes together with an increased areal nuclei

number density (**Fig. 4b – 4f**). At a low current rate of 0.05 mAh cm^{-2}, the Li deposits appear as irregular-shaped clusters with a size in the range of tens of microns, likely due to the fusing of multiple Li nuclei at such low current density. When the current rate increases from 0.2 to 1.0 mA cm^{-2}, the size of Li nuclei reduces (average nuclei size of ~10, ~ 8 and ~ 6 μm at 0.2, 0.5 and 1.0 mA cm^{-2}, respectively) but the areal number density of the nuclei grows gradually; meanwhile, the nuclei size distribution becomes increasingly more homogeneous and the nuclei shape appears increasingly more spherical. These observations are supported by the inverse relationship between the critical nuclei radius and the overpotential of Li deposition [70] and are also in agreement with the Li nuclei growth mechanism reported in ref. [71]. When the current density further increases to 2.0 mA cm^{-2}, no further reduction in the Li nuclei size is observed; whereas most of the Li nuclei turn into open hollow spheres, and as a result, the nuclei number density grows and the mass density drops, which may imply that the growth of the Li nuclei initiates with a thin toroid and progresses inward. It should also be noted that the Li deposits grow homogeneously on the nickel honeycomb skeleton within the 3D porous host which can be attributed to the homogeneous ionic charge distribution and low current density on the porous nickel current collector. This uniform Li nucleation benefits from the presence of numerous conductive nickel tips on the honeycomb-like skeleton, all of which function as nucleation sites and charge centres for Li deposition and thus the charge localization in just one or few points has been avoided. As a result, Li nucleates and grows evenly on the nickel host and fills the pores of the 3D porous current collector, and can be expected to form a relatively even Li surface.

To further investigate the Li nucleation and growth mechanism in the 3D nickel host, various amounts of Li were deposited at a current density of 1.0 mA cm^{-2}, as shown in **Fig. 4e** & **4g – 4k**. From 0.2 to 0.5 mAh cm^{-2}, the Li nuclei appear as spheres with a size of around 5 μm, and the areal number density of Li nuclei rises when the capacity increases. It is also observed that

the initial Li nucleation mostly takes place in the pores of the 3D nickel structure rather than on the top surface of the nickel layer. This may be attributed to: (i), the fact that the initial nucleation is not limited by any Li^+ ion depletion of the electrolyte, and (ii), the nickel walls of the honeycomb are multi-branched exhibiting numerous nickel tips in the pores of the 3D nickel host and limited amount of nickel tips on the top surface of the nickel layer, therefore, there are many more sites for Li nucleation in the pores than on top of the nickel layer. After nucleation the subsequent Li plating continues predominantly at all these nuclei in the pores. When the capacity of Li deposition grows to ≥ 1.0 mAh cm^{-2}, the size of Li nuclei grows, because after the initial Li nucleation, it is more energetically favourable for the following Li plating to take place on the initial Li nuclei rather than on the nickel skeleton. It is also observed that the Li nuclei become at larger sizes surface-cracked, possibly induced by the rising internal stress with the increasing capacity. With further Li deposition above 3.0 mAh cm^{-2}, the nuclei fill up the honeycomb pores and may even grow out of the nickel structure and fuse with their neighbouring nuclei. The entire nickel layer is homogeneously covered by Li deposits when the areal capacity reaches about 5.0 mAh cm^{-2}.

Based on the analysis above, an outline of the Li deposition progression mechanism is illustrated by **Fig. 4l**. In comparison, the Li grown on a planar Cu foil (**Fig. S12**) shows discrete island-like deposits, which is highly inhomogeneous, establishing the significantly positive effects of the 3D nickel structure for the suppression of Li dendrites. The dendritic Li growth on a planar Cu current collector occurs because the initial Li deposition nuclei function as the charge centres for additional Li nucleation and thus the subsequent Li deposition takes place on these sharp edges and induces the dendritic Li growth.

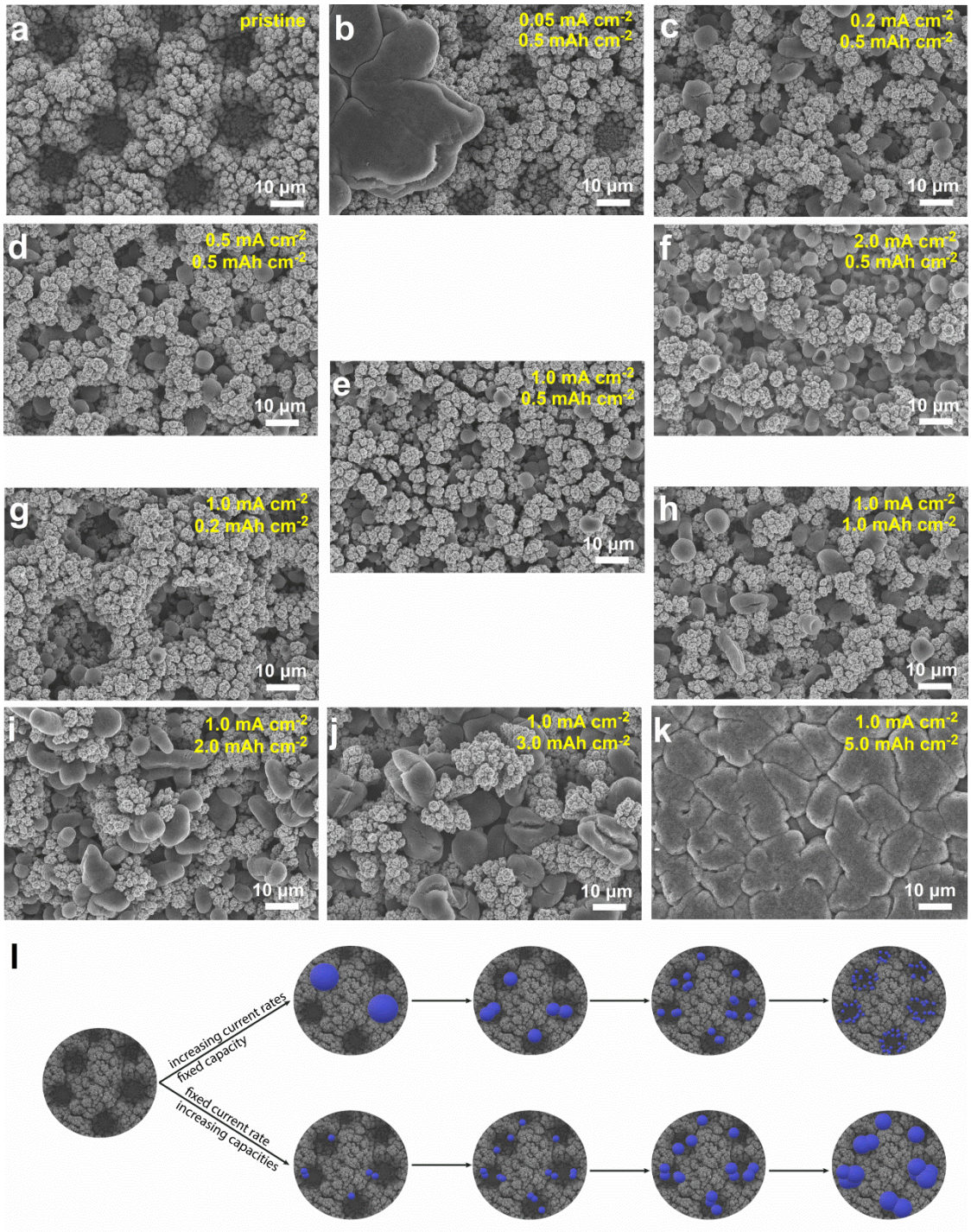

Fig. 4. Mechanisms of Li plating in the 3D Ni@Cu structure in a LiTFSI based electrolyte with 1 wt. % $LiNO_3$. (a) – (f), SEM images of the 3D Ni@Cu with 0.5 mAh cm^{-2} Li deposited under varying current densities from 0.05 to 2.0 mA cm^{-2}; (e) and (g) – (k), micrographs of the 3D Ni@Cu with different amounts of Li deposits cycling at 1.0 mA cm^{-2}. (l), a schematic illustrating the Li deposit growing mechanism in the 3D Ni@Cu based on the micrographs in Fig. (a) – (k).

3.3 Na plating performance

The promising cycling performance of 3D Ni@Cu on Li deposition/dissolution encouraged us to explore its potential for the reversible Na plating and stripping, which was characterized using 3D Ni@Cu as the working electrode and Na metal as the counter electrode.

Fig. 5a shows that, generally, compared to bare Cu foil, 3D Ni@Cu exhibits a much improved cycling stability and lifespan for Na plating/stripping. The porous conductive current collector achieves an exceptional cycling stability with a Coulombic efficiency of > 99.5 % for over 220 cycles cycling at a current density of 1.0 mA cm^{-2} for a capacity of 0.5 mAh cm^{-2}; when the Na deposition capacity increases to 1.0 and 2.0 mAh cm^{-2}, 3D Ni@Cu can still obtain a stable cycling performance for approximately 110 and 50 cycles, respectively.

Fig. 5b - 5c shows the galvanostatic voltage profiles of the bare Cu and 3D Ni@Cu for Na deposition and dissolution. It shows that the voltage hysteresis between charge and discharge grows continuously over cycling with a planar Cu current collector (~ 11 and 23 mV at 1^{st} and 100^{th} cycle, respectively); whereas 3D Ni@Cu exhibits stable overpotential (~ 17 mV) after the initial cycle. The initial voltage hysteresis of the 3D Ni@Cu is relatively higher, which is probably associated with a higher activation energy barrier of the porous nickel skeleton for Na nucleation owing to higher thermodynamic costs of forming a critical cluster of Na atoms on the nanosized nickel tips compared to a smooth Cu foil.

Morphological evolution of initial Na deposition on the 3D nickel current collector (**Fig. 5d – 5f**) reveals the Na plating mechanism in the porous nickel host. It illustrates that the Na deposits initially grow in some of the vertical pores of the honeycomb structure and gradually progress horizontally when the capacity increases; vertical growth (thickening) of Na deposition layer is evidenced as well. Fusing of Na deposits takes place when the Na deposits evolve and meet the neighbouring ones, and, eventually, a flat-surface Na anode (i.e. dendrite-

free deposition) is obtained. The Na plating occurs uniformly throughout the current collector area and is superior to the inhomogeneous Na growth on a planar Cu foil (**Fig. S13**), thanks to the beneficial nano/micro-morphological features of these 3D conductive structures enabling non-dendritic Li deposition as explained above. It is interesting that the sodium deposition appears to be even more uniform than Li deposits at a current density of 1.0 mA cm^{-2}, which can be attributed to the advantageous $NaPF_6$/DEGDME electrolyte that has been reported to help to suppress the dendritic Na growth [53].

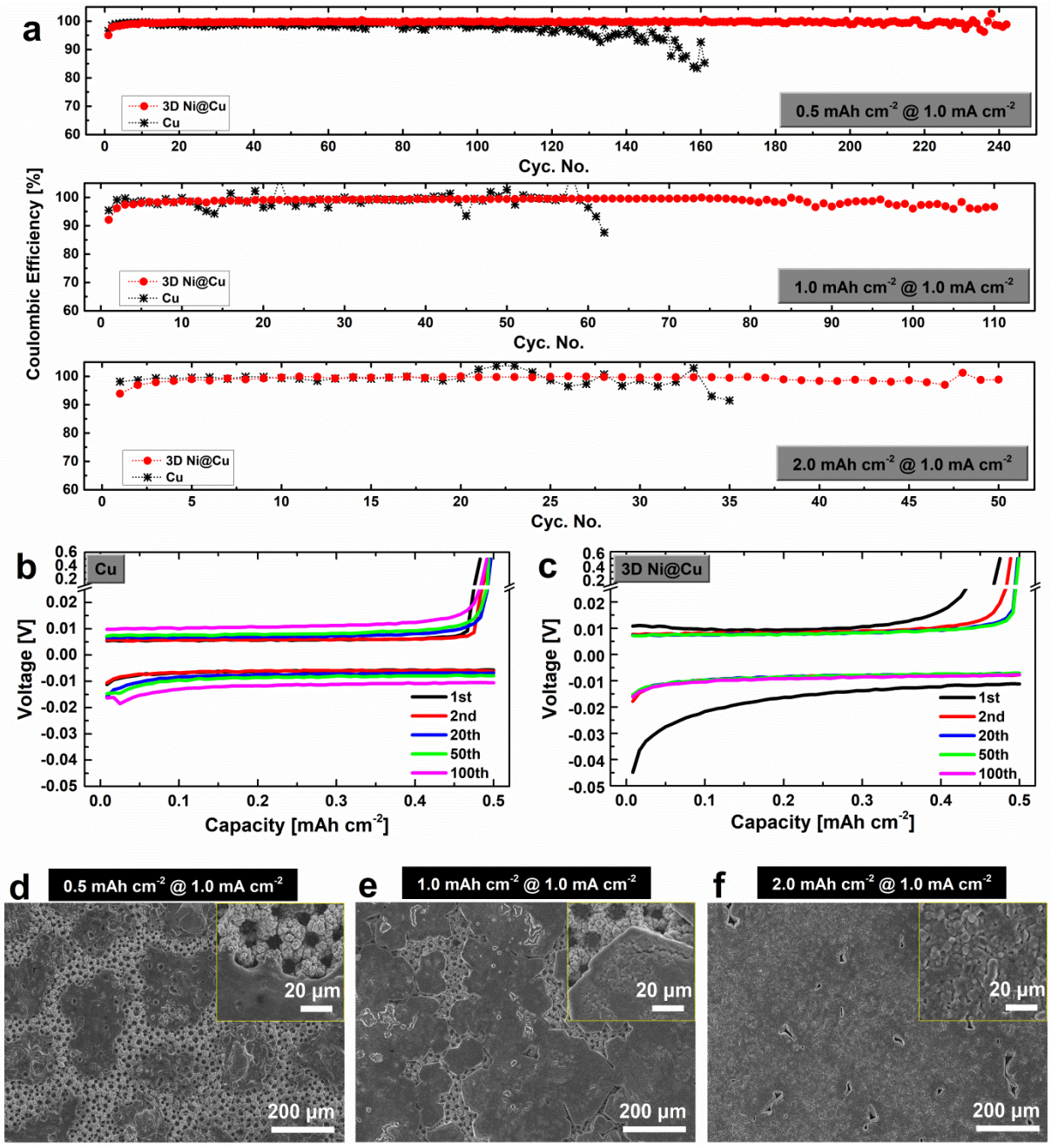

Fig. 5. Performance of the 3D Ni@Cu for Na plating/stripping at 1.0 mA cm^{-2}. (a), cycling performance with different areal capacities; (b), voltage profiles of the planar Cu electrode; (c), voltage response of 3D Ni@Cu electrode. (d) – (f), Morphologies of various amounts of Na deposited on 3D Ni@Cu.

4. Conclusions

We presented a facile one-step and low-cost synthesis of 3D porous current collectors for stable Li/Na metal anodes. The 3D scaffolds developed here are reminiscent of a honeycomb, with hierarchically electrodeposited nickel nanoparticles building micro walls on a copper substrate. Although the presence of nickel in the 3D Ni@Cu current collector replaces some volume, it will not reduce the volumetric energy density of the electrode when compared to a dendritic porous Li deposition layer. This is because it facilitates remarkably homogeneous Li deposition fully filling its well defined porous structure that acts as a scaffold, leading to a highly stable cycling performance. Addition of $LiNO_3$ to the electrolyte can effectively suppress the SEI formation and improve the Coulombic efficiency, and thus prolongs the lifespan of battery cycling. These current collectors also offer excellent cycling performance of Na plating/stripping with higher Columbic efficiently and stability. Moreover, this straight-forward process of 3D porous Ni@Cu scaffolds can in principle be extended to other application domains by adjusting the electrodeposition parameters. Therefore, considering the ease of our method for fabricating 3D current collectors, new insights into Li/Na plating-stripping and role of electrolyte additive promoting a robust solid electrolyte interface (SEI), our results provide promising solutions to expedite the implementation of Li/Na metal based high energy density batteries.

5. Appendix. Supporting Information

The supporting information contains the synthesis details of nickel electrodeposition, characteristics and the performance for Li plating/stripping of nickel electrodepositions with

modified fabrication conditions, and discussions on the porosity of the structure. XRD and XPS studies on the electrodes using electrolytes with and without $LiNO_3$ are included, and SEM images of the Li/Na deposition on planar Cu and 3D Ni@Cu are also provided.

Acknowledgement

This work was supported by A green Deal in Energy Materials (ADEM) grant funded by Dutch Ministry of Economic Affairs and ADEM industrial partners. A. S. Menon acknowledges financial support from the TNO - Holst Centre. We also thank Dr. Chandramohan George at TU Delft for the proofreading and comments on the manuscript.

References

[1] H. Kim, G. Jeong, Y.-U. Kim, J.-H. Kim, C.-M. Park, H.-J. Sohn, Metallic anodes for next generation secondary batteries, Chem. Soc. Rev. 42 (2013) 9011-9034.

[2] X.-B. Cheng, R. Zhang, C.-Z. Zhao, Q. Zhang, Toward Safe Lithium Metal Anode in Rechargeable Batteries: A Review, Chem. Rev. 117 (2017) 10403–10473 .

[3] D. Lin, Y. Liu, Y. Cui, Reviving the lithium metal anode for high-energy batteries, Nat. Nanotechnol. 12 (2017) 194-206.

[4] J. Lang, L. Qi, Y. Luo, H. Wu, High performance lithium metal anode: Progress and prospects, Energy Storage Mater. 7 (2017) 115-129.

[5] W. Xu, J. Wang, F. Ding, X. Chen, E. Nasybulin, Y. Zhang, J.-G. Zhang, Lithium metal anodes for rechargeable batteries, Energy Environ. Sci. 7 (2014) 513-537.

[6] B.L. Ellis, L.F. Nazar, Sodium and sodium-ion energy storage batteries, Curr. Opin. Solid State Mater. Sci. 16 (2012) 168-177.

[7] W. Luo, L. Hu, Na Metal Anode: “Holy Grail” for Room-Temperature Na-Ion Batteries?, ACS Cent. Sci. 1 (2015) 420-422.

[8] J.-Y. Hwang, S.-T. Myung, Y.-K. Sun, Sodium-ion batteries: present and future, Chem. Soc. Rev. 46 (2017) 3529-3614.

[9] K.N. Wood, M. Noked, N.P. Dasgupta, Lithium Metal Anodes: Toward an Improved Understanding of Coupled Morphological, Electrochemical, and Mechanical Behavior, ACS Energy Lett. 2 (2017) 664-672.

[10] K. Liu, A. Pei, H.R. Lee, B. Kong, N. Liu, D. Lin, Y. Liu, C. Liu, P.-c. Hsu, Z. Bao, Y. Cui, Lithium Metal Anodes with an Adaptive "Solid-Liquid" Interfacial Protective Layer, J. Am. Chem. Soc. 139 (2017) 4815-4820.

[11] G. Zheng, S.W. Lee, Z. Liang, H.-W. Lee, K. Yan, H. Yao, H. Wang, W. Li, S. Chu, Y. Cui, Interconnected hollow carbon nanospheres for stable lithium metal anodes, Nat. Nanotechnol. 9 (2014) 618-623.

[12] A.C. Kozen, C.-F. Lin, O. Zhao, S.B. Lee, G.W. Rubloff, M. Noked, Stabilization of Lithium Metal Anodes by Hybrid Artificial Solid Electrolyte Interphase, Chem. Mater. 29 (2017) 6298-6307.

[13] J.-S. Kim, D.W. Kim, H.T. Jung, J.W. Choi, Controlled Lithium Dendrite Growth by a Synergistic Effect of Multilayered Graphene Coating and an Electrolyte Additive, Chem. Mater. 27 (2015) 2780-2787.

[14] X. Liang, Q. Pang, I.R. Kochetkov, M.S. Sempere, H. Huang, X. Sun, L.F. Nazar, A facile surface chemistry route to a stabilized lithium metal anode, Nat. Energy 6 (2017) 17119.

[15] L. Wang, L. Zhang, Q. Wang, W. Li, B. Wu, W. Jia, Y. Wang, J. Li, H. Li, Long lifespan lithium metal anodes enabled by Al_2O_3 sputter coating, Energy Storage Mater. (2017).

[16] Y. Zhang, J. Qian, W. Xu, S.M. Russell, X. Chen, E. Nasybulin, P. Bhattacharya, M.H. Engelhard, D. Mei, R. Cao, F. Ding, A.V. Cresce, K. Xu, J.-G. Zhang, Dendrite-Free Lithium Deposition with Self-Aligned Nanorod Structure, Nano Lett. 14 (2014) 6889-6896.

[17] J. Park, J. Jeong, Y. Lee, M. Oh, M.-H. Ryou, Y.M. Lee, Micro-Patterned Lithium Metal Anodes with Suppressed Dendrite Formation for Post Lithium-Ion Batteries, Adv. Mater. Interfaces 3 (2016) 1600140.

[18] D. Lin, Y. Liu, Z. Liang, H.-W. Lee, J. Sun, H. Wang, K. Yan, J. Xie, Y. Cui, Layered reduced graphene oxide with nanoscale interlayer gaps as a stable host for lithium metal anodes, Nat. Nanotechnol. 11 (2016) 626-632.

[19] B. Li, D. Zhang, Y. Liu, Y. Yu, S. Li, S. Yang, Flexible Ti_3C_2 MXene-lithium film with lamellar structure for ultrastable metallic lithium anodes, Nano Energy 39 (2017) 654-661.

[20] X.-B. Cheng, C. Yan, H.-J. Peng, J.-Q. Huang, S.-T. Yang, Q. Zhang, Sulfurized solid electrolyte interphases with a rapid Li^+ diffusion on dendrite-free Li metal anodes, Energy Storage Mater. (2017).

[21] Y. Liu, D. Lin, Z. Liang, J. Zhao, K. Yan, Y. Cui, Lithium-coated polymeric matrix as a minimum volume-change and dendrite-free lithium metal anode, Nat. Commun. 7 (2016) 10992.

[22] C. Jin, O. Sheng, J. Luo, H. Yuan, C. Fang, W. Zhang, H. Huang, Y. Gan, Y. Xia, C. Liang, J. Zhang, X. Tao, 3D lithium metal embedded within lithiophilic porous matrix for stable lithium metal batteries, Nano Energy 37 (2017) 177-186.

[23] Z. Liang, D. Lin, J. Zhao, Z. Lu, Y. Liu, C. Liu, Y. Lu, H. Wang, K. Yan, X. Tao, Y. Cui, Composite lithium metal anode by melt infusion of lithium into a 3D conducting scaffold with lithiophilic coating, Proc. Natl. Acad. Sci. 113 (2016) 2862-2867.

[24] L.-L. Lu, Y. Zhang, Z. Pan, H.-B. Yao, F. Zhou, S.-H. Yu, Lithiophilic Cu–Ni core–shell nanowire network as a stable host for improving lithium anode performance, Energy Storage Mater. 9 (2017) 31-38.

[25] A. Zhang, X. Fang, C. Shen, Y. Liu, C. Zhou, A carbon nanofiber network for stable lithium metal anodes with high Coulombic efficiency and long cycle life, Nano Res. 9 (2016) 3428-3436.

[26] Y. Zhang, B. Liu, E. Hitz, W. Luo, Y. Yao, Y. Li, J. Dai, C. Chen, Y. Wang, C. Yang, H. Li, L. Hu, A carbon-based 3D current collector with surface protection for Li metal anode, Nano Res. 10 (2017) 1356-1365.

[27] Z. Zhang, X. Xu, S. Wang, Z. Peng, M. Liu, J. Zhou, C. Shen, D. Wang, Li2O-Reinforced Cu Nanoclusters as Porous Structure for Dendrite-Free and Long-Lifespan Lithium Metal Anode, ACS Appl. Mater. Interfaces 8 (2016) 26801-26808.

[28] Q. Li, S. Zhu, Y. Lu, 3D Porous Cu Current Collector/Li-Metal Composite Anode for Stable Lithium-Metal Batteries, Adv. Funct. Mater. 27 (2017) 1606422.

[29] C.-P. Yang, Y.-X. Yin, S.-F. Zhang, N.-W. Li, Y.-G. Guo, Accommodating lithium into 3D current collectors with a submicron skeleton towards long-life lithium metal anodes, Nat. Commun. 6 (2015) 8058.

[30] Q. Yun, Y.-B. He, W. Lv, Y. Zhao, B. Li, F. Kang, Q.-H. Yang, Chemical Dealloying Derived 3D Porous Current Collector for Li Metal Anodes, Adv. Mater. 28 (2016) 6932-6939.

[31] L.-L. Lu, J. Ge, J.-N. Yang, S.-M. Chen, H.-B. Yao, F. Zhou, S.-H. Yu, Free-Standing Copper Nanowire Network Current Collector for Improving Lithium Anode Performance, Nano Lett. 16 (2016) 4431-4437.

[32] K. Xie, W. Wei, K. Yuan, W. Lu, M. Guo, Z. Li, Q. Song, X. Liu, J.-G. Wang, C. Shen, Toward Dendrite-Free Lithium Deposition via Structural and Interfacial Synergistic Effects of 3D Graphene@Ni Scaffold, ACS Appl. Mater. Interfaces 8 (2016) 26091-26097.

[33] H.-K. Kang, S.-G. Woo, J.-H. Kim, J.-S. Yu, S.-R. Lee, Y.-J. Kim, Few-Layer Graphene Island Seeding for Dendrite-Free Li Metal Electrodes, ACS Appl. Mater. Interfaces 8 (2016) 26895-26901.

[34] X.-B. Cheng, T.-Z. Hou, R. Zhang, H.-J. Peng, C.-Z. Zhao, J.-Q. Huang, Q. Zhang, Dendrite-Free Lithium Deposition Induced by Uniformly Distributed Lithium Ions for Efficient Lithium Metal Batteries, Adv. Mater. 28 (2016) 2888-2895.

[35] W. Liu, D. Lin, A. Pei, Y. Cui, Stabilizing Lithium Metal Anodes by Uniform Li-Ion Flux Distribution in Nanochannel Confinement, J. Am. Chem. Soc. 138 (2016) 15443-15450.

[36] S.-S. Chi, Y. Liu, W.-L. Song, L.-Z. Fan, Q. Zhang, Prestoring Lithium into Stable 3D Nickel Foam Host as Dendrite-Free Lithium Metal Anode, Adv. Funct. Mater. 27 (2017) 1700348.

[37] R. Zhang, X.-R. Chen, X. Chen, X.-B. Cheng, X.-Q. Zhang, C. Yan, Q. Zhang, Lithiophilic Sites in Doped Graphene Guide Uniform Lithium Nucleation for Dendrite-Free Lithium Metal Anodes, Angew. Chem. Int. Ed. 56 (2017) 7764-7768.

[38] S. Matsuda, Y. Kubo, K. Uosaki, S. Nakanishi, Insulative Microfiber 3D Matrix as a Host Material Minimizing Volume Change of the Anode of Li Metal Batteries, ACS Energy Lett. 2 (2017) 924-929.

[39] M.D. Tikekar, S. Choudhury, Z. Tu, L.A. Archer, Design principles for electrolytes and interfaces for stable lithium-metal batteries, Nat. Energy 1 (2016) 16114.

[40] R. Miao, J. Yang, X. Feng, H. Jia, J. Wang, Y. Nuli, Novel dual-salts electrolyte solution for dendrite-free lithium-metal based rechargeable batteries with high cycle reversibility, J. Power Sources 271 (2014) 291-297.

[41] J. Guo, Z. Wen, M. Wu, J. Jin, Y. Liu, Vinylene carbonate–$LiNO_3$: A hybrid additive in carbonic ester electrolytes for SEI modification on Li metal anode, Electrochem. Commun. 51 (2015) 59-63.

[42] E. Markevich, G. Salitra, F. Chesneau, M. Schmidt, D. Aurbach, Very Stable Lithium Metal Stripping–Plating at a High Rate and High Areal Capacity in Fluoroethylene Carbonate-Based Organic Electrolyte Solution, ACS Energy Lett. 2 (2017) 1321-1326.

[43] W. Li, H. Yao, K. Yan, G. Zheng, Z. Liang, Y.-M. Chiang, Y. Cui, The synergetic effect of lithium polysulfide and lithium nitrate to prevent lithium dendrite growth, Nat. Commun. 6 (2015) 7436.

[44] J. Qian, W.A. Henderson, W. Xu, P. Bhattacharya, M. Engelhard, O. Borodin, J.-G. Zhang, High rate and stable cycling of lithium metal anode, Nat. Commun. 6 (2015) 6362.

[45] J. Shim, H.J. Kim, B.G. Kim, Y.S. Kim, D.-G. Kim, J.-C. Lee, 2D boron nitride nanoflakes as a multifunctional additive in gel polymer electrolytes for safe, long cycle life and high rate lithium metal batteries, Energy Environ. Sci. (2017), DOI: 10.1039/c7ee01095h.

[46] X.-Q. Zhang, X.-B. Cheng, X. Chen, C. Yan, Q. Zhang, Fluoroethylene Carbonate Additives to Render Uniform Li Deposits in Lithium Metal Batteries, Adv. Funct. Mater. 27 (2017) 1605989.

[47] C.-Z. Zhao, X.-B. Cheng, R. Zhang, H.-J. Peng, J.-Q. Huang, R. Ran, Z.-H. Huang, F. Wei, Q. Zhang, Li_2S_5-based ternary-salt electrolyte for robust lithium metal anode, Energy Storage Mater. 3 (2016) 77-84.

[48] K. Liu, D. Zhuo, H.-W. Lee, W. Liu, D. Lin, Y. Lu, Y. Cui, Extending the Life of Lithium-Based Rechargeable Batteries by Reaction of Lithium Dendrites with a Novel Silica Nanoparticle Sandwiched Separator, Adv. Mater. 29 (2017) 1603987.

[49] W.-K. Shin, A.G. Kannan, D.-W. Kim, Effective Suppression of Dendritic Lithium Growth Using an Ultrathin Coating of Nitrogen and Sulfur Codoped Graphene Nanosheets on Polymer Separator for Lithium Metal Batteries, ACS Appl. Mater. Interfaces 7 (2015) 23700-23707.

[50] Y. Liu, Q. Liu, L. Xin, Y. Liu, F. Yang, E.A. Stach, J. Xie, Making Li-metal electrodes rechargeable by controlling the dendrite growth direction, Nat. Energy 2 (2017) 17083.

[51] J.-N. Chazalviel, Electrochemical aspects of the generation of ramified metallic electrodeposits, Phys. Rev. A 42 (1990) 7355-7367.

[52] C. Brissot, M. Rosso, J.-N. Chazalviel, S. Lascaud, Dendritic growth mechanisms in lithium/polymer cells, J. Power Sources 81 (1999) 925-929.

[53] Z.W. Seh, J. Sun, Y. Sun, Y. Cui, A Highly Reversible Room-Temperature Sodium Metal Anode, ACS Cent. Sci. 1 (2015) 449-455.

[54] R. Cao, K. Mishra, X. Li, J. Qian, M.H. Engelhard, M.E. Bowden, K.S. Han, K.T. Mueller, W.A. Henderson, J.-G. Zhang, Enabling room temperature sodium metal batteries, Nano Energy 30 (2016) 825-830.

[55] J. Song, G. Jeong, A.-J. Lee, J.H. Park, H. Kim, Y.-J. Kim, Dendrite-Free Polygonal Sodium Deposition with Excellent Interfacial Stability in a $NaAlCl_4$–$2SO_2$ Inorganic Electrolyte, ACS Appl. Mater. Interfaces 7 (2015) 27206-27214.

[56] W. Luo, C.-F. Lin, O. Zhao, M. Noked, Y. Zhang, G.W. Rubloff, L. Hu, Ultrathin Surface Coating Enables the Stable Sodium Metal Anode, Adv. Energy Mater. 7 (2017) 1601526.

[57] Y. Zhao, L.V. Goncharova, A. Lushington, Q. Sun, H. Yadegari, B. Wang, W. Xiao, R. Li, X. Sun, Superior Stable and Long Life Sodium Metal Anodes Achieved by Atomic Layer Deposition, Adv. Mater. 29 (2017) 1606663.

[58] Y.-J. Kim, H. Lee, H. Noh, J. Lee, S. Kim, M.-H. Ryou, Y.M. Lee, H.-T. Kim, Enhancing the Cycling Stability of Sodium Metal Electrodes by Building an Inorganic–Organic Composite Protective Layer, ACS Appl. Mater. Interfaces 9 (2017) 6000-6006.

[59] W. Luo, Y. Zhang, S. Xu, J. Dai, E. Hitz, Y. Li, C. Yang, C. Chen, B. Liu, L. Hu, Encapsulation of Metallic Na in an Electrically Conductive Host with Porous Channels as a Highly Stable Na Metal Anode, Nano Lett. 17 (2017) 3792-3797.

[60] A.P. Cohn, N. Muralidharan, R. Carter, K. Share, C.L. Pint, Anode-Free Sodium Battery through in Situ Plating of Sodium Metal, Nano Lett. 17 (2017) 1296-1301.

[61] B.J. Plowman, L.A. Jones, S.K. Bhargava, Building with bubbles: the formation of high surface area honeycomb-like films via hydrogen bubble templated electrodeposition, Chem. Commun. 51 (2015) 4331-4346.

[62] J.-H. Kim, R.-H. Kim, H.-S. Kwon, Preparation of copper foam with 3-dimensionally interconnected spherical pore network by electrodeposition, Electrochem. Commun. 10 (2008) 1148-1151.

[63] S.S. Zhang, Role of $LiNO_3$ in rechargeable lithium/sulfur battery, Electrochim. Acta 70 (2012) 344-348.

[64] S.S. Zhang, A new finding on the role of $LiNO_3$ in lithium-sulfur battery, J. Power Sources 322 (2016) 99-105.

[65] W. Jia, C. Fan, L. Wang, Q. Wang, M. Zhao, A. Zhou, J. Li, Extremely Accessible Potassium Nitrate (KNO_3) as the Highly Efficient Electrolyte Additive in Lithium Battery, ACS Appl. Mater. Interfaces 8 (2016) 15399–15405.

[66] X.-B. Cheng, R. Zhang, C.-Z. Zhao, F. Wei, J.-G. Zhang, Q. Zhang, A Review of Solid Electrolyte Interphases on Lithium Metal Anode, Adv. Sci. 3 (2016) 1500213.

[67] M.R. Busche, T. Drossel, T. Leichtweiss, D.A. Weber, M. Falk, M. Schneider, M.-L. Reich, H. Sommer, P. Adelhelm, J. Janek, Dynamic formation of a solid-liquid electrolyte interphase and its consequences for hybrid-battery concepts, Nat. Chem. 8 (2016) 426-434.

[68] R. Dedryvère, S. Leroy, H. Martinez, F. Blanchard, D. Lemordant, D. Gonbeau, XPS Valence Characterization of Lithium Salts as a Tool to Study Electrode/Electrolyte Interfaces of Li-Ion Batteries, J. Phys. Chem. B 110 (2006) 12986-12992.

[69] D. Aurbach, E. Pollak, R. Elazari, G. Salitra, C.S. Kelley, J. Affinito, On the Surface Chemical Aspects of Very High Energy Density, Rechargeable Li–Sulfur Batteries, J. Electrochem. Soc. 156 (2009) A694-A702.

[70] D.R. Ely, R.E. García, Heterogeneous Nucleation and Growth of Lithium Electrodeposits on Negative Electrodes, J. Electrochem. Soc. 160 (2013) A662-A668.

[71] A. Pei, G. Zheng, F. Shi, Y. Li, Y. Cui, Nanoscale Nucleation and Growth of Electrodeposited Lithium Metal, Nano Lett. 17 (2017) 1132-1139.